Article

Vadlazarenkovite, $Pd_8Bi_{1.5}Te_{1.25}As_{0.25}$, a new mineral isotypic with mertieite from the Konder massif, Far East, Russia

Anatoly V. Kasatkin[1]*, Cristian Biagioni[2], Fabrizio Nestola[3], Atali A. Agakhanov[1], Sergey Yu. Stepanov[4], Vladislav V. Gurzhiy[5], Sergey V. Petrov[5], and Andrey G. Pilugin[6]

[1]Fersman Mineralogical Museum of the Russian Academy of Sciences, Leninsky Prospekt 18-2, 119071 Moscow, Russia;

[2]Dipartimento di Scienze della Terra, Università di Pisa, Via Santa Maria 53, I-56126 Pisa, Italy;

[3]Dipartimento di Geoscienze, Università di Padova, Via Gradenigo 6, I-35131, Padova, Italy;

[4]South Urals Federal Research Center of Mineralogy and Geoecology UB RAS, 456317, Miass, Chelyabinsk district, Russia;

[5]Institute of Earth Sciences, St. Petersburg State University, University Emb. 7/9, 199034 Saint-Petersburg, Russia;

[6]LLC "Nornickel Technical Services", Grazhgdanskiy Prospekt 11, 195 220, Saint-Petersburg, Russia

*Author for correspondence: Anatoly V. Kasatkin, E-mail: anatoly.kasatkin@gmail.com

Running title: Vadlazarenkovite, a new mineral

Abstract

The new mineral vadlazarenkovite, ideally $Pd_8Bi_{1.5}Te_{1.25}As_{0.25}$, was discovered in a heavy concentrate obtained from ore samples collected at the Anomal'noe occurrence, Konder alkaline-ultrabasic massif, Khabarovsk Krai, Far East, Russia. It occurs as anhedral grains up to 0.15 × 0.15 mm intergrown with vysotskite and associates with numerous platinum-group elements (PGE) bearing minerals (arsenopalladinite, ezochiite, hollingworthite, kotulskite, norilskite, polarite, skaergaardite, sobolevskite, sperrylite, törnroosite, zvyagintsevite etc.). Vadlazarenkovite is grey, opaque with metallic luster, brittle tenacity and uneven fracture. No cleavage and parting are observed. The Vickers' micro-indentation

This is a 'preproof' accepted article for Mineralogical Magazine. This version may be subject to change during the production process.
DOI: 10.1180/mgm.2024.52

hardness (VHN, 50 g load) is 424 kg/mm^2 (range 406–443, n = 4), corresponding to a Mohs' hardness of 4.5–5. $D_{calc.}$ = 11.947 g/cm^3. In reflected light, vadlazarenkovite is white with pale creamy hue. The bireflectance is weak in air and noticeable in oil immersion. In crossed nicols the new mineral exhibits distinct anisotropy in grey tones. The reflectance values for wavelengths recommended by the Commission on Ore Mineralogy of the International Mineralogical Association are (R_{min}/R_{max}, %): 47.2/47.8 (470 nm), 49.1/50.8 (546 nm), 50.7/52.6 (589 nm) and 52.4/54.6 (650 nm). The chemical composition (wt.%, electron microprobe data, mean of 6 analyses) is: Pd 63.67, Ag 2.21, As 1.27, Sb 0.60, Te 11.26, Pb 2.56, Bi 19.95, total 101.51. The empirical formula calculated on the basis of 11 atoms per formula unit is $(Pd_{7.87}Ag_{0.27})_{\Sigma 8.14}(Bi_{1.26}Te_{1.16}As_{0.22}Pb_{0.16}Sb_{0.06})_{\Sigma 2.86}$. Vadlazarenkovite is trigonal, space group $R\bar{3}c$, a = 7.7198(2), c = 43.1237(11) Å, V = 2225.66(13) Å^3 and Z = 12. The strongest lines of the X-ray powder diffraction pattern [*d,* Å (*I*, %) (*hkl*)] are: 2.308 (55) (1 1 15), 2.262 (100) (2 0 14), 2.232 (70) (3 0 0), 2.040 (70) (1 1 18). The crystal structure of vadlazarenkovite was refined to R_1 = 0.0267 for 761 reflections with $F_o > 4\sigma(F_o)$. The new mineral is isotypic with mertieite. It honors Professor Vadim Grigorievich Lazarenkov (1933–2014) for his outstanding contributions to the geology, geochemistry and mineralogy of platinum-group elements.

Keywords: vadlazarenkovite; new mineral; platinum-group elements; chemical composition; crystal structure; mertieite; Anomal'noe occurrence; Konder massif; Russia

Introduction

In the course of the study by scanning electron microscopy with energy-dispersive spectrometry (SEM-EDS), ore microscopy and single-crystal X-ray diffraction (SCXRD) of a heavy concentrate obtained from ore samples collected at the Konder alkaline-ultrabasic massif, Khabarovsk Krai, Far East, Russia (57° 35' 12" N, 134° 39' 9" E), the senior author of the present paper encountered an array of rare PGE-bearing minerals. Amongst them one unknown phase gave essential Pd, Bi, Te, minor Ag, As, Sb and Pb at SEM-EDS and unit-cell parameters similar to the mineral mertieite-II, ideally $Pd_8Sb_{2.5}As_{0.5}$ (Karimova *et al.*, 2018), later renamed to mertieite by the Commission on New Minerals, Nomenclature and Classification (CNMNC) of the International Mineralogical Association (IMA) (Miyawaki *et al.*, 2022). Further investigations showed this phase to be a new mineral isotypic to mertieite. It was named vadlazarenkovite in the honor of Professor Vadim Grigorievich Lazarenkov (Вадим Григорьевич Лазаренков) (1933–2014), Soviet and Russian scientist who worked at the Saint-Petersburg Mining University, for his outstanding contributions to the geology and petrology of ultrabasic and basic rocks, including those from the Konder deposit, as well as to the geochemistry and mineralogy of PGE (see, *e.g.*, Lazarenkov and Malich, 1992; Lazarenkov *et al.*, 1992; Lazarenkov and Talovina, 2001; Lazarenkov *et al.*, 2002 *etc.*). The name "vadlazarenkovite" was preferred to "lazarenkovite" to avoid confusion with the

https://doi.org/10.1180/mgm.2024.52 Published online by Cambridge University Press

existing mineral lazarenkoite, $CaFe^{3+}As^{3+}{}_3O_7 \cdot 3H_2O$ (Yakhontova and Plusnina, 1981). The new mineral, its name and symbol (Vlz) have been approved by the CNMNC of the IMA (IMA2023–040, Kasatkin *et al.*, 2023). The holotype specimen is deposited in the systematic collection of the Fersman Mineralogical Museum of the Russian Academy of Sciences, Moscow, with the catalogue number 98319.

To date, the Konder massif was the type locality of four mineral species – konderite (Rudashevskiy *et al.*, 1984), cuproiridsite (Rudashevskiy *et al.*, 1985), bortnikovite (Mochalov *et al.*, 2007) and ferhodsite (Begizov and Zavyalov, 2016). All of them contain PGE as species-defining components. Thus, vadlazarenkovite is the fifth new mineral discovered there.

Occurrence and general appearance

The Konder (alternative spelling – Kondyor) massif is located at the Eastern margin of the Aldan shield within a sub-latitudinal zone of a Proterozoic continental rift. This zone crosses the Batomga ledge of the crystalline basement at its intersection with the Konder-Netsky sublongitudinal fault (Gurovich *et al.*, 1994). The massif is composed of Early-Proterozoic rocks of the Konder dunite-clinopyroxenite-gabbro complex and Early-Cretaceous rocks of the Ketkap monzodiorite plutonic complex (Dymovich *et al.*, 2012) and represents a subvertical diapir (or stock) with almost perfectly circular projection, which is bounded by circular faults (Fig. 1). The Konder massif has a concentrically-zoned structural pattern and is composed of a dunite core (diameter 5.1–6 km, area 24.7 km^2) and a relatively thin (up to 850 m in thickness) rim of clinopyroxenites, ore clinopyroxenites (kosvites) and gabbros. Dunite body is zoned as well, and its zonation is manifested in a transition of fine-grained to medium- and coarse-grained varieties through porphyric ones. The Konder massif is a source of one of the World largest placer deposits of platinum (Lazarenkov *et al.*, 2002). Since its exploration had begun in 1984, more than 106 tons of platinum has been recovered from the related placers (Pilyugin and Bugaev, 2016). This deposit is also renowned for discoveries of many large platinum nuggets (Mochalov, 2019).

Lately, presumably economic PGE concentrations have been established in veins of zeolite- and amphibole-bearing phlogopite clinopyroxenites, which host fine-grained copper sulfide mineralization. Drilling prospection of a complex Cu-Pt-Pd geochemical and magnetic geophysical anomaly in 2013–2014 revealed a Cu-Pt-Pd ore occurrence named Anomal'noe (Gurevich and Polonyankin, 2016; Pilyugin and Bugaev, 2016). Geological structure of this mineralized area is characterized by a broad presence of Ti-magnetite clinopyroxenites with the related metasomatic rocks (Fig. 2), which always cross-cut dunites and form a stockwork in western and central parts of the dunite core. The largest bodies of Ti-magnetite clinopyroxenites strike subhorizontally or slightly dipping. These clinopyroxenites are rich in phlogopite (that could be the late-stage one) and have coarse-grained sideronitic and, occasionally, breccia-like textures. Cu-Pt-Pd mineralization is localized exclusively within veins, composed by phlogopite, clinopyroxene and zeolites. These veins are steeply dipping, have relatively small length (up to 100–200

https://doi.org/10.1180/mgm.2024.52 Published online by Cambridge University Press

m) and thickness (1–4 m on average). Copper sulfides mainly include fine-grained segregations of bornite, chalcopyrite and chalcocite. PGE-bearing minerals coexist with copper sulfides and form isolated inclusions of small size (0.12 mm on average). The latter usually represent complex intergrowths of different PGE-bearing minerals: intermetallic compounds, sulfides, arsenides and tellurides. According to authors' data, palladium concentration in the veins is up to 63.7 g/t, platinum – up to 33.7 g/t, gold – 1.3 g/t and silver – more than 100 g/t.

More detailed description of the Konder massif, its geology and mineralogy can be found elsewhere (Gurovich *et al.*, 1994; Cabri and Laflamme, 1997; Malich, 1999; Shcheka *et al.*, 2004; Simonov *et al.*, 2011; Tolstykh, 2018; Mochalov, 2019 *etc.*).

Vadlazarenkovite was found in a heavy concentrate obtained from ore samples collected at the Anomal'noe ore occurrence during field works at the deposit in 2014–2018. The new mineral occurs as anhedral grains up to 0.15 × 0.15 mm intergrown with vysotskite, ideally PdS (Fig. 3). Associated PGE-bearing minerals include arsenopalladinite, cooperite, ezochiite, hollingworthite, isomertieite, kotulskite, laurite, malanite, norilskite, polarite, Zn-bearing skaergaardite, sobolevskite, sperrylite, stillwaterite, törnroosite, tulameenite, vysotskite, and zvyagintsevite. Several PGE-bearing phases in the same association are unknown and are currently under investigation. Other associated minerals include anilite, bornite, chalcocite, chalcopyrite, chromite, cubanite, digenite, galena, Cr-bearing magnetite, silver, stromeyerite and phlogopite.

Vadlazarenkovite is extremely rare: only two grains of the mineral have been found so far, 0.15 × 0.15 mm and 0.05 × 0.01 mm.

Physical properties and optical data

Vadlazarenkovite is grey, opaque with metallic luster, brittle tenacity and uneven fracture. It does not fluoresce under ultraviolet light. No cleavage and parting are observed. The Vickers' micro-indentation hardness (VHN, 50 g load) is 424 kg/mm^2 (range 406–443, n = 4), corresponding to a Mohs' hardness of 4.5–5. Density could not be measured due to the very small amount of available material and absence of necessary heavy liquids. A density value calculated using the empirical formula and the unit-cell parameters from SCXRD data is 11.947 g cm^{-3}.

In reflected light, vadlazarenkovite is white with pale creamy hue. The bireflectance is weak in air and noticeable in oil immersion. No pleochroism or internal reflections were observed. In crossed nicols the new mineral exhibits distinct anisotropy in grey tones. Reflectance values have been measured in air using an MSF-R (LOMO, Saint-Petersburg, Russia) microspectrophotometer. Silicon was used as a standard. The reflectance values (R_{max}/R_{min}) are given in Table 1 and plotted in Fig. 4 in comparison with the published data for mertieite (Cabri, 1981). Note that reflectance curves of both minerals have close resemblance with a clearly defined dispersion of anomalous type, however, for vadlazarenkovite the

https://doi.org/10.1180/mgm.2024.52 Published online by Cambridge University Press

minimum is in the violet part of the spectrum (420 nm), while for mertieite it is shifted to the right, into the blue region (450 nm).

Chemical Data

Chemical data (six spot analyses) were collected with a Tescan Solari FEG-SEM equipped with WDS Wave 700 Oxford Instruments (25 kV, 10 nA, 2 μm beam size). Contents of other elements with atomic numbers > 4 are below detection limits. Matrix correction by PAP algorithm (Pouchou and Pichoir, 1985) was applied to the data. Analytical data and list of standards are given in Table 2.

The empirical formula calculated on the basis of 11 atoms per formula unit is $(Pd_{7.87}Ag_{0.27})_{\Sigma 8.14}(Bi_{1.26}Te_{1.16}As_{0.22}Pb_{0.16}Sb_{0.06})_{\Sigma 2.86}$. The ideal formula of vadlazarenkovite, considering the results of the crystal structure analysis (see below), is $Pd_8Bi_{1.5}Te_{1.25}As_{0.25}$, which requires (in wt.%) Pd 63.39, Bi 23.34, Te 11.88, As 1.39, total 100.

X-ray Crystallography and Crystal Structure

Powder X-ray diffraction (PXRD) data were collected using a Rigaku R-AXIS Rapid II single-crystal diffractometer equipped with a cylindrical image plate detector (radius 127.4 mm) using Debye-Scherrer geometry, Co*K*α radiation (rotating anode with VariMAX microfocus optics), 40 kV and 15 mA. Angular resolution of the detector is 0.045° 2θ (pixel size 0.1 mm). The data were integrated using the software package *Osc2Tab* (Britvin *et al.*, 2017). PXRD data of vadlazarenkovite are given in Table 3 in comparison to that calculated from SCXRD data using the *PowderCell*2.3 software (Kraus and Nolze, 1996). Parameters of trigonal unit cell were calculated from the observed *d* spacing data using *UnitCell* software (Holland and Redfern, 1997) and are as follows: a = 7.722(4), c = 43.11(4) Å, and V = 2226(2) Å^3. It should be noted that due to the lack of material, PXRD data were collected from the same grain which was used for SCXRD studies (see below). This issue with the preferential orientation of the single crystal during PXRD data collection also introduces a difference in the intensity of the peaks in the observed and calculated powder diffraction patterns while maintaining their angular positions (Table 3).

For the SCXRD study, a grain of vadlazarenkovite, 0.024 × 0.020 × 0.016 mm^3 in size, extracted from the polished section analysed using electron microprobe (Fig. 3), was mounted on a glass fiber and examined through a Supernova Rigaku-Oxford Diffraction diffractometer equipped with a micro-source Mo*K*α radiation (λ = 0.71073 Å; 50 kV, 0.8 mA) and a Pilatus 200K Dectris detector. The data were processed by CrysAlisPro 1.171.41.123a software (Rigaku Oxford Diffraction) and are as follows: vadlazarenkovite is trigonal, space group $R\bar{3}c$, a = 7.7198(2), c = 43.1237(11) Å, V = 2225.66(13) Å^3 and Z = 12. Intensity data were collected using φ scan modes, in 1° slices, the sample-to-detector distance was set to 69 mm, with an exposure time of 25 s per frame. A total of 1689 frames over 30 runs were collected for a total time of about 12 hours. Data were corrected for Lorentz-polarization, absorption, and

https://doi.org/10.1180/mgm.2024.52 Published online by Cambridge University Press

background. Unit-cell parameters were refined on the basis of the XYZ centroids of 5028 reflections with $3 < \theta < 31.7$ °.

The crystal structure of vadlazarenkovite was refined using Shelxl-2018 (Sheldrick, 2015) starting from the atomic coordinates of mertieite (Karimova *et al.*, 2018). The following neutral scattering curves, taken from the *International Tables for Crystallography* (Wilson, 1992), were used: Pd at Pd1-Pd4 sites, Bi at Bi1 (Sb1 in Karimova *et al.*, 2018), Te at *M*1 and *M*2 (*M*1 and As1 in Karimova *et al.*, 2018). Several cycles of isotropic refinement converged to $R_1 = 0.1016$, thus confirming the correctness of the structural model. At this stage of the refinement, the U_{iso} value at the *M*1 site was too low, suggesting the occurrence of heavier atoms. Consequently, the site occupancy at this position was refined using the scattering curves of Bi *vs*. Te. The refinement improved to $R_1 = 0.0815$. After several cycles of anisotropic refinement, the R_1 factor converged to 0.0416. At this stage, the site occupancies at Bi1 and *M*2 were refined, using the scattering curves of Bi *vs*. □ and Te *vs*. □, respectively. The Bi1 and *M*2 sites were found to be occupied by lighter atoms, and in the final stage of the refinement, their site occupancies were refined using the scattering curves of Bi *vs*. Te and Te *vs*. As, respectively. Owing to the similar scattering factors of Bi ($Z = 83$) and Pb ($Z = 82$), and of Te ($Z = 52$), Sb ($Z = 51$), and Ag ($Z = 47$), the actual distribution of Pb, Sb, and Ag in the crystal structure of vadlazarenkovite was only hypothesized and these elements were not included in the refinement. The final anisotropic structural model converged to $R_1 = 0.0267$ for 761 reflections with $F_o > 4\sigma(F_o)$ and 39 refined parameters. Details of data collection and refinement are given in Table 4. Fractional atom coordinates and equivalent isotropic displacement parameters are reported in Table 5. Table 6 reports selected interatomic distances. The crystallographic information file has been deposited with the Principal Editor of Mineralogical Magazine and is available as Supplementary material (see below).

Vadlazarenkovite's crystal structure (Fig. 5) has four symmetry-independent Pd sites at 36*f* (Pd1 and Pd2) and 12*c* (Pd3 and Pd4) positions. Atom coordinations are shown in Figure 6. Palladium atoms at Pd1 are coordinated to 8 Pd atoms, with distances ranging between 2.85 and 3.18 Å, and to four (Bi/Te)-bearing sites. At the Pd2 site, Pd atoms are coordinated by nine Pd atoms (in the interatomic distance range of 2.87-3.21 Å) and four (Bi/Te/As)-hosting sites. Pd3 and Pd4 have 13 and 11 neighbours, respectively. The former is characterized by nine Pd–Pd contacts shorter than 3.20 Å and four Pd–(Bi/Te/As) distances, whereas the latter displays seven Pd–Pd interatomic distances shorter than 3 Å and four (Bi/Te) contacts. Table 7 reports a comparison between coordination numbers and average values of Pd–Pd and Pd–Me (Me = As, Bi, Sb, and Te) distances in vadlazarenkovite, mertieite (Karimova *et al.*, 2018), and synthetic Pd_8Sb_3 (Wopersnow and Schubert, 1976; Marsh, 1994). It is worth noting that Pd–Me distances are larger than those observed in mertieite; this is keeping with the replacement of Sb and As by larger Bi atoms. At the four Pd sites, no evidence for the occurrence of other elements other than

https://doi.org/10.1180/mgm.2024.52 Published online by Cambridge University Press

Pd was observed during the crystal structure refinement. However, the possible occurrence of minor Ag cannot be discarded.

The Bi1 site (Wyckoff position 18*e*) has coordination number 12; the mean atomic number (MAN) at this position is 74.66 electrons, indicating the partial replacement of Bi by lighter atoms (likely Te and minor Sb). In mertieite, this site was fully occupied by Sb (Karimova *et al.*, 2018). The *M*1 site (at the 12*c* position) is ten-fold coordinated by Pd atoms, and its refined MAN is 66.38 electrons, thus indicating the possible mixed Bi/Te occupancy of this site. In mertieite, this 12*c* position was occupied by Sb, with minor As ($Sb_{0.94}As_{0.06}$ in crystal I and $Sb_{0.88}As_{0.12}$ in crystal II). Finally, the *M*2 site, at the position 6*b*, is eight-fold coordinated by Pd atoms and its refined mean atomic number (MAN = 43.20 electrons) agrees with a mixed Te/As site. Taking into account the site multiplicity, the refined site scattering at the Bi1, *M*1, and *M*2 sites is 199.97 electrons per formula unit ($Z = 12$). This value has to be compared with the results of electron microprobe analysis, i.e., $Pd_{7.87(5)}Ag_{0.27(1)}Bi_{1.26(20)}Te_{1.16(18)}As_{0.22(3)}Pb_{0.16(2)}Sb_{0.06(1)}$. Assuming that minor Ag replaces Pd at the Pd sites, the site population at the Bi1+*M*1+*M*2 sites would be $Bi_{1.26}Te_{1.16}As_{0.22}Pb_{0.16}Ag_{0.14}Sb_{0.06}$, corresponding to 194.92 electrons.

A difficult task is represented by the actual description of the element partitioning among the Me-bearing sites. The largest Me atoms (i.e., Ag, Pb) could be attributed to the Bi1 site, along with Sb (in agreement with what observed in mertieite, where Sb is preferentially partitioned there with respect to *M*1 and As1 – Karimova *et al.*, 2018). Consequently, Bi1 could have an idealized site population (considering the site multiplicity and the refined MAN) close to $Bi_{0.90}Te_{0.25}Pb_{0.15}Ag_{0.15}Sb_{0.05}$.

The *M*1 site could be considered as a mixed Bi/Te site. Refined MAN agrees with $Te_{0.55}Bi_{0.45}$. However, considering also the chemical data, a Te/Bi atomic ratio close to 1.5 seems to be reasonable, i.e., $Te_{0.60}Bi_{0.40}$.

Finally, the *M*2 site is a mixed Te/As site. Refined MAN and electron microprobe data allow us to suggest the population $Te_{0.25}As_{0.25}$.

The proposed structural formula of vadlazarenkovite is $^{Pd1\text{-}Pd4}Pd_8{}^{Bi1}Bi_{1.5}{}^{M1}Te_{1.00}{}^{M2}(Te_{0.25}As_{0.25})$, i.e., $Pd_8Bi_{1.5}Te_{1.25}As_{0.25}$ ($Z = 12$).

Discussion

Crystal chemical features

Vadlazarenkovite, $Pd_8Bi_{1.5}Te_{1.25}As_{0.25}$, is isotypic with mertieite, $Pd_8Sb_{2.5}As_{0.5}$ (Karimova *et al.*, 2018; Miyawaki *et al.*, 2022). For the comparison of the two species see Table 8. Synthetic Pd_8Bi_3 was reported by Sarah and Schubert (1979), with unit-cell parameters $a = 7.81$, $c = 42.60$ Å, space group *R*3.

As shown in Table 2, vadlazarenkovite has a relatively large range of Te and Bi contents. In agreement with the result of crystal structure analysis we assumed the following substitutions:

i) Pd is replaced by minor Ag at Pd1-Pd4 sites;

https://doi.org/10.1180/mgm.2024.52 Published online by Cambridge University Press

ii) Bi is replaced by minor Pb, Ag, Sb, and possibly Te at the Bi1 site;

iii) Te is replaced by Bi at the *M*1 site;

iv) Te and As occur at the *M*2 site.

Following these substitution rules, the following chemical formulae can be written for the six spot analyses:

1) $(Pd_{7.83}Ag_{0.17})(Bi_{1.12}Pb_{0.14}Ag_{0.10}Sb_{0.07}Te_{0.06})(Te_{1.00})(Te_{0.27}As_{0.23})$;

2) $(Pd_{7.88}Ag_{0.12})(Bi_{1.11}Pb_{0.17}Ag_{0.16}Sb_{0.06})(Te_{0.74}Bi_{0.26})(Te_{0.26}As_{0.24})$;

3) $(Pd_{7.91}Ag_{0.09})(Bi_{1.10}Pb_{0.16}Ag_{0.17}Sb_{0.06})(Te_{0.93}Bi_{0.07})(Te_{0.27}As_{0.23})$;

4) $(Pd_{7.91}Ag_{0.09})(Bi_{1.11}Pb_{0.17}Ag_{0.15}Sb_{0.06})(Te_{0.86}Bi_{0.14})(Te_{0.28}As_{0.22})$;

5) $(Pd_{7.78}Ag_{0.22})(Bi_{1.17}Pb_{0.19}Ag_{0.07}Sb_{0.07})(Te_{0.59}Bi_{0.41})(Te_{0.34}As_{0.16})$;

6) $(Pd_{7.87}Ag_{0.13})(Bi_{1.05}Pb_{0.14}Ag_{0.15}Sb_{0.06}Te_{0.10})Te_{1.00}(Te_{0.26}As_{0.24})$.

In all cases, Bi is dominant at Bi1, Te at *M*1, whereas *M*2 site population is close to $Te_{0.25}As_{0.25}$. This latter mixed (Te/As) occupancy, with a Te/As atomic ratio close to one, may be due to geochemical constraints or may indicate a possible role of the $(Te_{0.5}As_{0.5})$ double-site occupancy in the stabilization of vadlazarenkovite.

Geochemical features

The platinum-group mineral assemblage found at the Anomal'noe occurrence is characteristic of copper sulfide (chalcopyrite, chalcopyrite-bornite and bornite) ores, hosted by gabbroic rocks of the Ural-Alaskan type, which are found both in fold belts and cratons. The first include gabbro massifs of the Northern Urals (Stepanov *et al.*, 2020; Mikhailov *et al.*, 2021), Koryak Highlands (Kutyrev *et al.*, 2021; Palyanova *et al.*, 2023) and Alaska (Milidragovic *et al.*, 2021). The second are represented by Inagli and Gulinskiy massifs (Sazonov *et al.*, 2021; Chayka *et al.*, 2023) and Konder described in this paper.

An important feature of the copper-PGE mineralization at Anomal'noe is the wide occurrence of PGE-bearing minerals containing Bi, Te and Pb. One of these is vadlazarenkovite that contains Bi and Te as species-defining elements and Pb as a minor constituent. The absence of Bi, Te and Pb in PGE-bearing minerals or their extreme rarity in rocks and ores of the zoned complexes of the fold belts can be explained by the fact that the latter were formed from magmas of the young ensimatic arc settings (Cai *et al.*, 2012; Habtoor *et al.*, 2016), where the content of Bi, Te and Pb in the geochemical systems is at a very low level. By contrast, formation of the Ural-Alaskan type complexes in cratons was likely accompanied by crustal assimilation that contributes typical crust-derived elements to the magmas. Although the contamination and, hence, enrichment of the magmas by these elements might be minor, it could be still enough to form such a unique PGE-bearing minerals assemblage.

Furthermore, for the case of the Anomal'noe occurrence, a role of the alkali-rich late magmatic fluids, emerged from the later stage Ketkap alkaline complex should be significant. Enriched with

https://doi.org/10.1180/mgm.2024.52 Published online by Cambridge University Press

phosphorus and fluorine, these fluids could re-deposit and concentrate ore metals (Gurevich, 2023) and produce the studied mineralization. Therefore, we suggest that the studied unique mineral assemblage, including vadlazarenkovite, was a result of the following superimposed factors: (1) contamination of mantle-derived rocks by crustal components, and (2) several stages of the metals' concentration with the aid of alkaline fluids derived from the subsequent magmatic pulse.

Supplementary material

To view supplementary material for this article, please visit: https://doi.org/...

Acknowledgements

We thank Associate Editor Owen Missen, František Laufek and two anonymous Reviewers for constructive comments that improved the manuscript. Ivan F. Chayka is acknowledged for the discussion on geological features and Maria D. Milshina – for the help with the figures. The PXRD studies have been performed at the Research Centre for X-ray Diffraction Studies of St. Petersburg State University within the framework of project AAAA-A19-119091190094-6.

References

Begizov V.D. and Zavyalov E.N. (2016) Ferhodsite $(Fe,Rh,Ir,Ni,Cu,Co,Pt)_{9-x}S_8$ – new mineral from Nizhny Tagil ultramafic complex. *Novye Dannye o Mineralakh (New Data on Minerals)*, **51**, 8–11 (in Russian).

Britvin S.N., Dolivo-Dobrovolsky D.V., Krzhizhanovskaya M.G. (2017) Software for processing the X-ray powder diffraction data obtained from the curved image plate detector of Rigaku RAXIS Rapid II diffractometer. *Zapiski Rossiiskogo Mineralogicheskogo Obshchestva*, **146**, 104–107 (in Russian).

Cabri L.J., Ed. (1981) Platinum-Group Elements: Mineralogy, Geology, Recovery. CIM Special Volume 23. The Canadian Institute of Mining and Metallurgy, 267 pp.

Cabri L.J. and Laflamme J.H.G. (1997) Platinum-group minerals from the Konder massif, Russian Far East. *Mineralogical Record*, **28**, 97–106.

Cai K., Sun M., Yuan C., Zhao G., Xiao W. and Long X. (2012) Keketuohai mafic-ultramafic complex in the Chinese Altai, NW China: petrogenesis and geodynamic significance. Chemical Geology, **294–295**, 26–41.

Chayka I.F., Kamenetsky V.S., Malitch K.N., Vasil'ev Y.R., Zelenski M.E., Abersteiner A.B. and Kuzmin I.A. (2023) Behavior of critical metals in cumulates of alkaline ultramafic magmas in the Siberian large igneous province: insights from melt inclusions in minerals. *Ore Geology Reviews*, 105577.

https://doi.org/10.1180/mgm.2024.52 Published online by Cambridge University Press

Dymovich V.A., Vas'kin A.F., Opalikhina E.S., Kislyakov S.G., Atrachenko A.F., Romanov B.I., Zelepugin V.N., Charov L.A. and Leontieva L.Yu. (2012) State geological map of Russian Federation, 1:10000000 (3rd edition). Far East series. Sheet O-53 – Nelkan. Explanatory note. VSEGEI Cartographic Factory, 364 p. (in Russian).

Gurevich D.V. (2023) Conder-Ketkap: two main stages in the formation of gold and PGM deposits – in: Gurevich D.V. and Polonyankin A.A. Scientific and methodological foundations of forecasting, prospecting, assessment of deposits of diamonds, precious and non-ferrous metals. Abstracts of the XIIth International Scientific and Practical Conference, Moscow, April 11–14, 2023. Moscow, Central Scientific Research Geological Prospecting Institute of Non-Ferrous and Precious Metals, 106-108 (in Russian).

Gurevich D.V. and Polonyankin A.A. (2016) Sulfide polymineral Pt-Pd ores of the Konder massif, Khabarovsk region: geological background. In: Proceedings of the all-Russian conference with international participation "Problems of geology and exploration of the platinum metals deposits (I scientific readings in memory of prof. V. G. Lazarenkov)". Mining University, Saint-Petersburg, p. 27–46 (in Russian).

Gurovich V.G., Emelyanenko E.P., Zemlyanukhin V.N., Karetnikov A.S., Kvasov A.I., Lazarenkov V.G., Malich K.N., Mochalov A.G., Prikhod'ko V.S. and Stepashko A.A. (1994) Geology, petrology and ore content of the Konder massif. Moscow, Nauka, 176 p. (in Russian).

Habtoor A., Ahmed A.H. and Harbi H. (2016) Petrogenesis of the Alaskan-type mafic-ultramafic complex in the Makkah quadrangle, western Arabian Shield, Saudi Arabia. *Lithos*, **263**, 33–51.

Holland T.J.B., Redfern S.A.T. (1997) Unit cell refinement from powder diffraction data: the use of regression diagnostics. *Mineralogical Magazine*, **61**, 65–77.

Karimova O.V., Zolotarev A.A., Evstigneeva T.L. and Johanson B.S. (2018) Mertieite-II, $Pd_8Sb_{2.5}As_{0.5}$, crystal-structure refinement and formula revision. *Mineralogical Magazine*, **82**, S247–S257.

Kasatkin A.V., Biagioni C., Nestola F., Agakhanov A.A., Stepanov S.Y., Petrov S.V. and Pilugin A.G. (2023) Vadlazarenkovite, IMA 2023–040. CNMNC Newsletter 75; *Mineralogical Magazine*, **87**,

Kraus W. and Nolze G. (1996) POWDER CELL – a program for the representation and manipulation of crystal structures and calculation of the resulting X-ray powder patterns. *Journal of Applied Crystallography*, **29**, 301–303.

Kutyrev A.V., Sidorov E.G., Kamenetsky V.S., Chubarov V.M., Chayka I.F. and Abersteiner A. (2021) Platinum mineralization and geochemistry of the Matysken zoned Ural-Alaskan type complex and related placer (Far East Russia). *Ore Geology Reviews*, **130**, 103947.

Lazarenkov V.G. and Malich K.N. (1992) Geochemistry of the ultrabasites of the Konder platiniferous massif. *Geochemistry International*, **29**(5), 44–56.

https://doi.org/10.1180/mgm.2024.52 Published online by Cambridge University Press

Lazarenkov V.G., Malich K.N. and Sakhyanov L.O. (1992) Platinum-metal mineralization of zonal ultrabasic and komatiite massifs. Leningrad, Nedra, 217 p. (in Russian).

Lazarenkov V.G. and Talovina I.V. (2001) Geochemistry of elements of the platinum group. Saint-Petersburg, Galart Publishing House, 266 p. (in Russian).

Lazarenkov V.G., Petrov S.V. and Talovina I.V. (2002) Deposits of platinum metals. Saint-Petersburg, Nedra, 298 p. (in Russian).

Malich K.N. (1999) Platinum group elements in clinopyroxenite-dunite massifs of the East Siberia (geochemistry, mineralogy and genesis). Saint-Petersburg cartographic factory VSEGEI, 296 p. (in Russian).

Marsh R.E. (1994) The centrosymmetric-noncentrosymmetric ambiguity: some more examples. *Acta Crystallographica*, **A50**, 450–455.

Mikhailov V.V., Stepanov S.Y., Kozlov A.V., Petrov S.V., Palamarchuk R.S., Shilovskikh V.V. and Abramova V.D. (2021) New copper–precious metal occurrence in gabbro of the Serebryansky Kamen massif, Ural platinum belt, Northern Urals. *Geology of Ore Deposits*, **63**(6), 528–555.

Milidragovic D., Nixon G.T., Scoates J.S., Nott J.A., Spence D.W. (2021) Redox-controlled chalcophile element geochemistry of the Polaris Alaskan-type mafic-ultramafic complex, British Columbia, Canada. *The Canadian Mineralogist*, **59**, 1627–1660.

Miyawaki R., Hatert F., Pasero M. and Mills S.J. (2022) IMA Commission on New Minerals, Nomenclature and Classification (CNMNC) – Newsletter 69. *European Journal of Mineralogy*, **34**. 463–468.

Mochalov A.G. (2019) Remarkable platinum minerals of the Konder massif (Khabarovsk Krai, Russia). *Mineralogical Almanac*, **23**(3), 128 p.

Mochalov A., Tolkachev M., Polekhovskiy Yu. and Goryacheva, E. (2007) Bortnikovite, Pd_4Cu_3Zn, a new mineral species from the unique Konder placer deposit, Khabarovsk krai, Russia. *Geologiya Rudnykh Mestorozhdenii (Geology of Ore Deposits),* **49**, 318–327 (in Russian).

Palyanova G., Kutyrev A., Beliaeva T., Shilovskikh V., Zhegunov P., Zhitova E. and Seryotkin Y. (2023) Pd, Hg-Rich Gold and Compounds of the Au-Pd-Hg System at the Itchayvayam Mafic-Ultramafic Complex (Kamchatka, Russia) and Other Localities. *Minerals*, **13**(4), 549.

Pilyugin A.G. and Bugaev I.A. (2016) Common problems of geology of copper-platinum-palladium mineralization of the Konder massif, Russian Far East. In: Proceedings of the all-Russian conference with international participation “Problems of geology and exploration of the platinum metals deposits (I scientific readings in memory of prof. V. G. Lazarenkov)”. Mining University, Saint-Petersburg, p. 22–26 (in Russian).

Pouchou J.L. and Pichoir F. (1985) “PAP” (jρZ) procedure for improved quantitative microanalysis. Pp. 104–106 in: *Microbeam Analysis* (J.T. Armstrong, editor). San Francisco Press, San Francisco.

https://doi.org/10.1180/mgm.2024.52 Published online by Cambridge University Press

Rudashevskiy N.S., Mochalov A.G., Trubkin N.V., Gorshkov A.I., Men'shikov Y.P. and Shumskaya N.I. (1984) Konderite $Cu_3Pb(Rh,Pt,Ir)_8S_{16}$ – a new mineral. *Zapiski Vserossiyskogo Mineralogicheskogo Obshchestva*, **113**, 703–712 (in Russian).

Rudashevskiy N.S., Men'shikov Yu.P., Mochalov A.G., Trubkin N.V., Shumskaya N.I., and Zhdanov V.V. (1985) Cuprorhodsite $CuRh_2S_4$ and cuproiridsite $CuIr_2S_4$ – new natural thiospinels of platinum-group elements. *Zapiski Vserossiyskogo Mineralogicheskogo Obshchestva*, **114**, 187–195 (in Russian).

Sarah N. and Schubert K. (1979) Kristallstruktur von Pd_5Bi_2. *Journal of the Less Common Metals*, **63**, P75–P82.

Sazonov A.M., Romanovsky A.E., Gertner I.F., Zvyagina E.A., Krasnova T.S., Grinev O.M. and Kolmakov Y.V. (2021) Genesis of precious metal mineralization in intrusions of ultramafic, alkaline rocks and carbonatites in the north of the Siberian platform. *Minerals*, **11**, 354.

Shcheka G.G., Lehmann B., Gierth E., Gömann K. and Wallianos A. (2004) Macrocrystals of Pt-Fe alloy from the Kondyor PGE placer deposit, Khabarovskiy kray, Russia: trace-element content, mineral inclusions and reaction assemblages. *The Canadian Mineralogist*, **42**, 601–617.

Sheldrick G.M. (2015) Crystal structure refinement with SHELXL. *Acta Crystallographica*, **C71**, 3–8.

Simonov V.A., Kovyazin S.V. and Prikhod'ko V.S. (2011) Genesis of platiniferous massifs in the Southeastern Siberian platform. *Petrology*, **19**(6), 549–567.

Stepanov S.Yu., Palamarchuk R.S., Antonov A.V., Kozlov A.V., Varlamov D.A., Khanin D.A. and Zolotarev Jr. A.A. (2020) Morphology, composition, and ontogenesis of platinum-group minerals in chromitites of zoned clinopyroxenite-dunite massifs of the Middle Urals. *Russian Geology and Geophysics*, **61**(1), 47–67.

Tolstykh N.D. (2018) Platinum mineralization of the Konder and Inagly massifs. *Geosphere Research*, **1**, 17–32 (in Russian).

Wilson A.J.C. (editor) (1992) *International Tables for Crystallography Volume C: Mathematical, Physical and Chemical Tables*. Kluwer Academic Publishers, Dordrecht, The Netherlands.

Wopersnow W. and Schubert K. (1976) Kristallstruktur von Pd_8Sb_3. *Journal of Less Common Metals*, **48**, 79-87.

Yakhontova L.K. and Plusnina I.I. (1981) The new mineral lazarenkoite. *Mineralogicheskiy Zhurnal*, **3**(3), 92–96 (in Russian with English abs.).

Table 1. Reflectance values for vadlazarenkovite (COM standard wavelengths are given in bold).

https://doi.org/10.1180/mgm.2024.52 Published online by Cambridge University Press

λ (nm)	R_{max}	R_{min}		λ (nm)	R_{max}	R_{min}
400	47.2	46.6		560	51.4	49.5
420	45.5	45.0		580	52.4	50.4
440	46.2	45.6		**589**	**52.6**	**50.7**
460	46.9	46.4		600	52.9	51.1
470	**47.8**	**47.2**		620	53.8	51.8
480	48.7	48.0		640	54.2	52.0
500	49.0	48.4		**650**	**54.6**	**52.4**
520	49.9	48.6		660	55.0	52.8
540	50.6	48.9		680	56.0	53.8
546	**50.8**	**49.1**		700	57.3	55.1

Table 2. Chemical data (in wt. %) and atoms per formula unit (apfu) for vadlazarenkovite.

	wt% (n = 6)			apfu			
Element	**Mean**	**Range**	**S.D.**	**Mean**	**Range**	**S.D.**	**Reference Material**
Pd	63.67	62.02 – 64.57	1.05	7.87	7.78 – 7.91	0.05	Pd
Ag	2.21	2.02 – 2.30	0.11	0.27	0.24 – 0.28	0.01	Ag
As	1.27	0.92 – 1.40	0.17	0.22	0.16 – 0.24	0.03	GaAs
Sb	0.60	0.56 – 0.69	0.05	0.06	0.06 – 0.07	0.01	Sb
Te	11.26	8.81 – 13.41	1.86	1.16	0.92 – 1.36	0.18	PbTe
Pb	2.56	2.25 – 3.01	0.28	0.16	0.14 – 0.19	0.02	PbTe
Bi	19.95	16.83 – 24.79	2.84	1.26	1.05 – 1.58	0.20	Bi
Total	101.51	100.29 – 102.46	0.78				

Table 3. Powder X-ray diffraction data (*d* in Å) of vadlazarenkovite.

d_{obs}	I_{obs}	d_{calc}*	I_{calc}*	*h k l*
3.726	7	3.728	9	1 1 3
3.400	5	3.401	11	1 1 6
2.795	10	2.798	5	0 1 14
2.641	5	2.642	7	0 2 10
2.528	16	2.523	10	2 1 1
2.334	15	2.338	5	2 1 7
2.308	**55**	**2.306**	**90**	1 1 15
2.262	**100**	**2.265**	**15**	2 0 14
2.232	**70**	**2.229**	**100**	3 0 0
2.040	**21**	**2.036**	**15**	1 1 18
1.954	10	1.954	11	1 2 14
1.605	10	1.602	15	2 2 15
1.504	8	1.503	5	2 2 18

* I_{calc}, d_{calc} were calculated using the *PowderCell2.3* software (Kraus and Nolze, 1996) on the basis of the structural model given in Table 5. Only reflections with $I_{calc} > 5$ are listed.
Strongest reflections are given in boldtype.

https://doi.org/10.1180/mgm.2024.52 Published online by Cambridge University Press

Table 4. Crystal and experimental data for vadlazarenkovite.

Crystal data	
Crystal size (mm)	0.024 × 0.020 × 0.016
Cell setting, space group	Trigonal, *R*-3*c*
a (Å)	7.7198(2)
c (Å)	43.1237(11)
V (Å^3)	2225.66(13)
Z	12
Data collection and refinement	
Radiation, wavelength (Å)	Mo *K*α, λ = 0.71073
Temperature (K)	293(2)
$2\theta_{max}$ (°)	63.48
Measured reflections	19886
Unique reflections	841
Reflections with $F_o > 4\sigma(F_o)$	761
R_{int}	0.0787
$R\sigma$	0.0259
Range of *h*, *k*, *l*	$-11 \le h \le 11$, $-11 \le k \le 11$, $-63 \le l \le 61$
R [$F_o > 4\sigma(F_o)$]	0.0267
R (all data)	0.0308
wR (on F_o^2)	0.0594
Goof	1.135
Number of least-squares parameters	39
Maximum and minimum residual peak (*e* Å^{-3})	2.90 [at 0.85 Å from *M*1] -1.71 [at 0.99 Å from *M*2]

https://doi.org/10.1180/mgm.2024.52 Published online by Cambridge University Press

Table 5. Site, site occupancy (s.o.), fractional atom coordinates, equivalent isotropic displacement parameters (Å^2) for vadlazarenkovite.

Site	Wyckoff Multiplicity	s.o.	*x*/*a*	*y*/*b*	*z*/*c*	U_{eq}
Pd1	36*f*	$Pd_{1.00}$	0.00190(8)	0.27291(11)	0.11545(2)	0.02286(18)
Pd2	36*f*	$Pd_{1.00}$	0.03097(9)	0.33497(8)	0.18379(2)	0.01826(16)
Pd3	12*c*	$Pd_{1.00}$	0	0	0.06030(2)	0.0211(2)
Pd4	12*c*	$Pd_{1.00}$	0	0	0.21762(2)	0.0170(2)
Bi1	18*e*	$Bi_{0.731(6)}Te_{0.269(6)}$	0.31903(5)	0	¼	0.01397(14)
*M*1	12*c*	$Te_{0.536(7)}Bi_{0.464(7)}$	0	0	0.15618(2)	0.01510(19)
*M*2	6*b*	$Te_{0.537(15)}As_{0.463(15)}$	0	0	0	0.0145(4)

Table 6. Selected interatomic distances (in Å) for vadlazarenkovite.

Pd1	– Bi1	2.7267(6)	Pd2	– *M*2	2.5640(5)
	– *M*1	2.7373(7)		– *M*1	2.7466(6)
	– Bi1	2.8309(6)		– *M*1	2.8206(6)
	– Pd4	2.8500(6)		– Bi1	2.8625(6)
	– Pd3	2.8570(7)		– Pd2	2.8653(7) × 2
	– Pd1	2.8859(11)		– Pd4	2.8728(7)
	– Pd2	2.9069(8)		– Pd1	2.9068(8)
	– Pd2	2.9417(8)		– Pd1	2.9416(8)
	– Pd2	2.9763(8)		– Pd1	2.9763(8)
	– Pd3	3.1726(11)		– Pd3	3.0811(9)
	– Pd2	3.1752(9)		– Pd1	3.1752(9)
	– Bi1	3.2987(7)		– Pd2	3.2118(17)
Pd3	– *M*2	2.6002(11)	Pd4	– *M*1	2.6494(10)
	– Bi1	2.8116(4) × 3		– Pd4	2.7928(17)
	– Pd1	2.8570(7) × 3		– Bi1	2.8312(5) × 3
	– Pd2	3.0812(9) × 3		– Pd1	2.8500(6) × 3
	– Pd1	3.1726(11) × 3		– Pd2	2.8728(7) × 3
Bi1	– Pd1	2.7268(6) × 2	*M*1	– Pd4	2.6494(10)
	– Pd3	2.8116(4) × 2		– Pd1	2.7372(7) × 3
	– Pd1	2.8310(6) × 2		– Pd2	2.7466(6) × 3
	– Pd4	2.8311(5) × 2		– Pd2	2.8206(6) × 3
	– Pd2	2.8626(6) × 2			
	– Pd1	3.2987(7) × 2			
*M*2	– Pd2	2.5639(5) × 6			

https://doi.org/10.1180/mgm.2024.52 Published online by Cambridge University Press

– Pd3 2.6001(11) × 2

https://doi.org/10.1180/mgm.2024.52 Published online by Cambridge University Press

Table 7. Comparison between average values of Pd–Pd and Pd–Me interatomic distances (in Å) in vadlazarenkovite, mertieite, and synthetic Pd_8Sb_3.

	Average distance with Pd atoms			Average distance with Me atoms		
Central atom	Vadlazarenkovite	Mertieite*	Pd_8Sb_3	Vadlazarenkovite	Mertieite*	Pd_8Sb_3
Pd1	2.971	2.996	3.053†/2.973††	2.898	2.835	2.860†/2.888††
Pd2	2.988	2.943	2.986†/3.012††	2.748	2.692	2.717†/2.742††
Pd3	3.037	2.966	3.008†/3.036††	2.759	2.710	2.732†/2.757††
Pd4	2.852	2.821	2.815†/2.844††	2.786	2.718	2.746†/2.768††
Bi1[a]	2.894	2.841	2.848†/2.874††			
*M*1	2.756	2.695	2.711†/2.738††			
*M*2[b]	2.573	2.500	2.613†/2.637††			

* Data after crystal I of Karimova *et al.* (2018).
† Data after Wopersnow and Schubert (1976).
†† Data after Marsh (1994).
[a] Sb1 in the crystal structure of mertieite (Karimova *et al.*, 2018).
[b] As1 in the crystal structure of mertieite (Karimova *et al.*, 2018).

Wopersnow W. and Schubert K

Table 8. Comparative data for vadlazarenkovite and mertieite.

Mineral	**Vadlazarenkovite**	**Mertieite**
Ideal formula	$Pd_8Bi_{1.5}Te_{1.25}As_{0.25}$	$Pd_8Sb_{2.5}As_{0.5}$*
Crystal system **Space group**	Trigonal $R\bar{3}c$	Trigonal* $R\bar{3}c$*
a, Å *c*, Å *V*, Å^3 *Z*	7.7198(2) 43.1237(11) 2225.66(13) 12	7.5172(3)* 43.037(2)* 2106.1(2)* 12*
Density (calc.), g cm^{-3}	11.947	11.287*
Vickers hardness, 50g load, kg mm^{-2}, mean (range)	424 (406–443)	544 (511–588)**
Optical properties: Colour in reflected light Bireflectance Pleochroism Anisotropy Internal reflections Reflectance values (COM)***	 White with pale creamy hue Weak None Distinct, in gray tones; very dark blue in partly crossed polars None 47.2/47.8; 49.1/50.8; 50.7/52.6; 52.4/54.6	 Creamy yellowish** None** None** Distinct, dark brownish gray to extinction** None** 45.2; 50.4; 52.7; 55.3***
Source	This paper	*Karimova *et al.* (2018) – data for crystal I

https://doi.org/10.1180/mgm.2024.52 Published online by Cambridge University Press

		**Cabri (1981) ***calculated from Cabri (1981)

***R_{max}/R_{min} for vadlazarenkovite, R' for mertieite

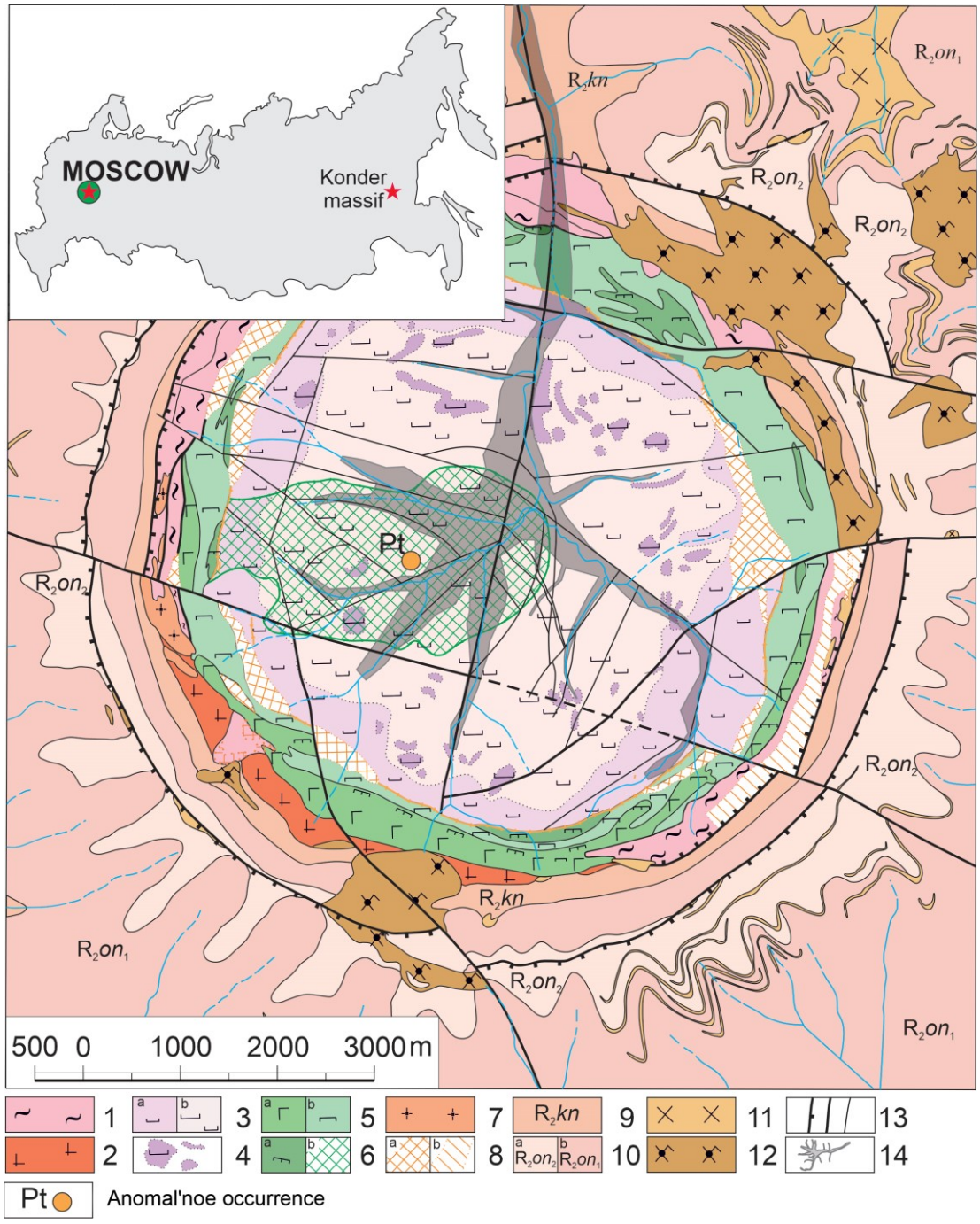

Figure 1. Geographical position (inset) and geological map of the Konder massif. 1 – crystalline schists, marbles, quartzites and gneisses of the Utukachan Formation (Ar_1ut), 2 – gneiss-like plagiogranites of the Hoyundin Formation ($p\gamma AR_1h$), 3 – dunites: (a) fine-grained and (b) porphyric, 4 – dunite pegmatites, 5 – mafic rocks: (a) gabbro, (b) clinopyroxenites, 6 – (a)

https://doi.org/10.1180/mgm.2024.52 Published online by Cambridge University Press

apatite-magnetite ore clinopyroxenites (kosvites) and (b) a stockwork of Ti-magnetite phlogopite clinopyroxenites with zeolites and copper sulfide mineralization, 7 – medium-alkaline pegmatoidal granites, 8 – metasomatites: (a) diopside-monticellite-garnet and diopside-forsterite metasomatites and (b) feldspar-clinopyroxene, 9 – siltstones, sandstones and gravelites of the Konder Formation, 10 – terrigeneous sedimentary rocks of the Omnin Formation of the lower (a) and upper (b) subformations, 11 – monzodiorites and monzonites of the Ketkap complex, 12 – quartz monzonites of the Ketkap complex, 13 – faults, 14 – industrial debris of the Konder Pt placer deposit.

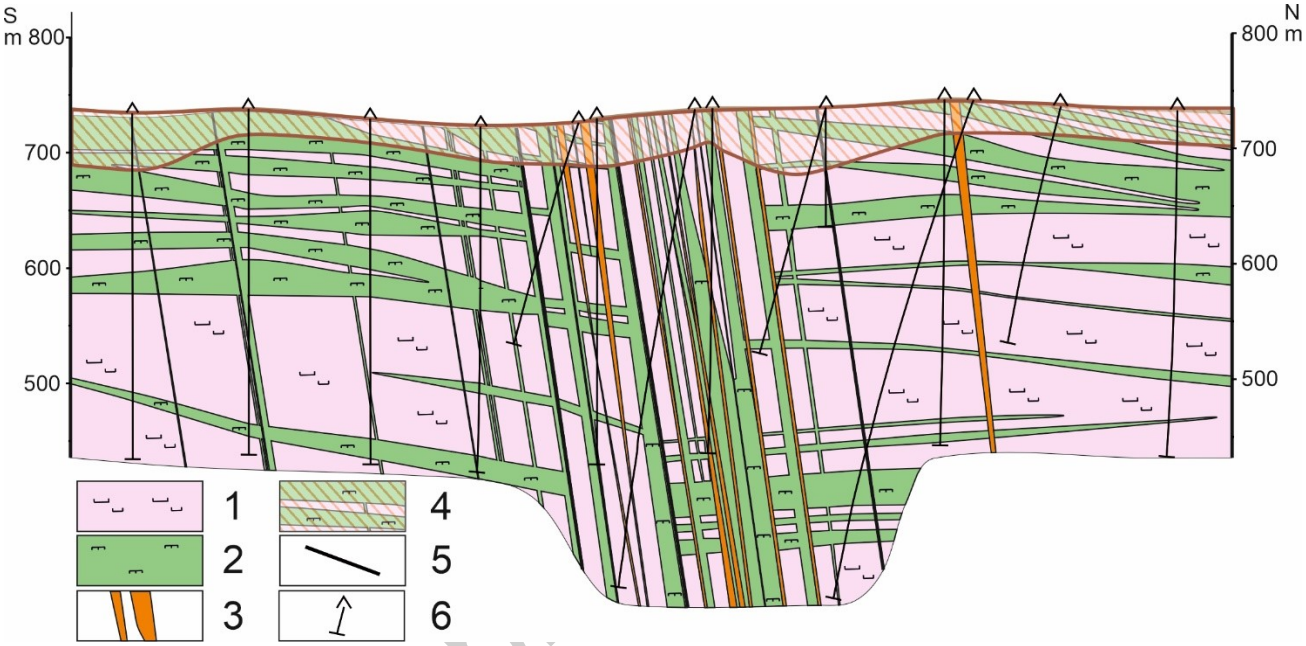

Figure 2. Cross-section of the central part of the Anomal'noe ore occurrence: 1 – porphyric dunites, 2 – Ti-magnetite clinopyroxenites equally-grained and porphyric, and their phlogopite and apatite varieties; 3 – vein of clinopyroxene-phlogopite, phlogopite, phlogopite-clinopyroxene and zeolite-clinopyroxene-phlogopite rocks; 4 – weathering crust after the bedrocks, 5 – faults, 6 – boreholes.

https://doi.org/10.1180/mgm.2024.52 Published online by Cambridge University Press

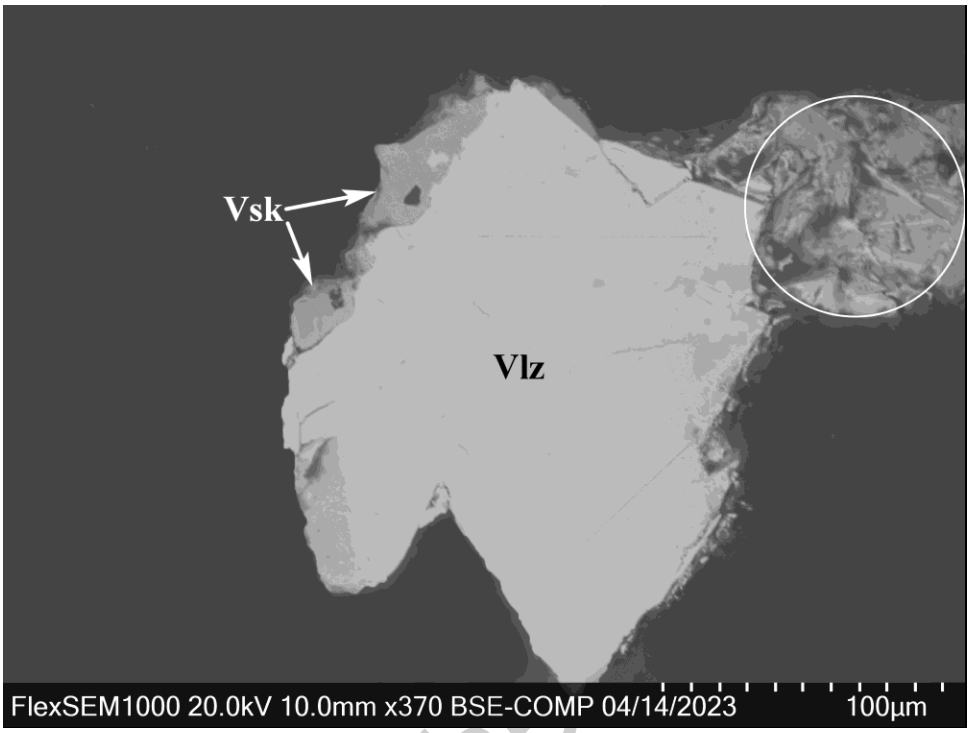

Figure 3. Vadlazarenkovite (Vlz) intergrown with vysotskite (Vsk). Part of this grain (in white circle) was extracted for structural studies. Polished section. SEM (BSE) image.

https://doi.org/10.1180/mgm.2024.52 Published online by Cambridge University Press

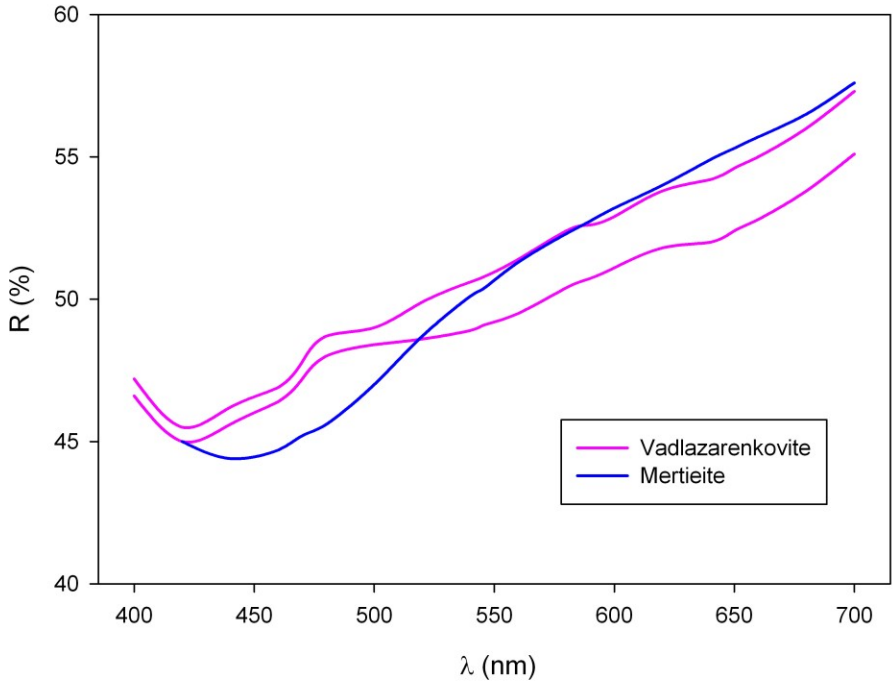

Figure 4. Reflectance curves of vadlazarenkovite in comparison with mertieite (Cabri, 1981).

https://doi.org/10.1180/mgm.2024.52 Published online by Cambridge University Press

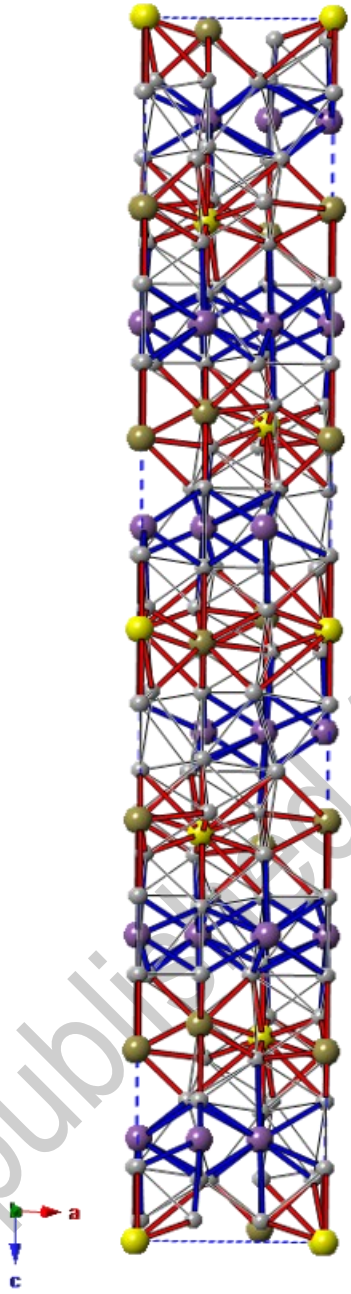

Figure 5. Unit-cell content of vadlazarenkovite as seen down **b**. Symbols: Pd sites are shown as grey circles, Bi1 site is represented by violet circles, and *M*1 and *M*2 sites are light brown and yellow circles, respectively. Pd–Bi and Pd–Te are shown as thick blue and red lines, respectively, whereas Pd–Pd contacts are shown as thin black lines.

https://doi.org/10.1180/mgm.2024.52 Published online by Cambridge University Press

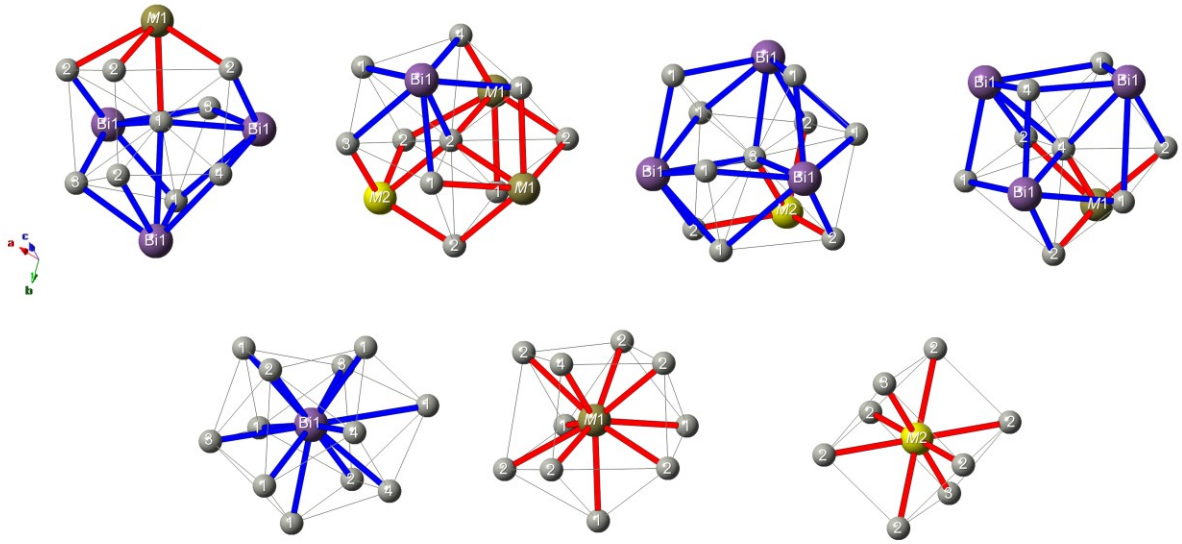

Figure 6. Coordination environments of atom sites in vadlazarenkovite. Same symbols as in Figure 5.

https://doi.org/10.1180/mgm.2024.52 Published online by Cambridge University Press